Ultralow longitudinal emittance storage rings

Y. Zhang, X. J. Deng, Z. L. Pan, Z. Z. Li, K. S. Zhou, W. H. Huang, R. K. Li, and C. X. Tang*

Department of Engineering Physics, Tsinghua University, Beijing 100084, China and Key Laboratory of Particle and Radiation Imaging, Tsinghua University, Ministry of Education, Beijing 100084, China

A. W. Chao

Institute for Advanced Study, Tsinghua University, Beijing 100084, China and Stanford University, Stanford, California 94309, USA

(Received 26 June 2021; accepted 26 August 2021; published 20 September 2021)

Low longitudinal emittance means small energy spread and short bunch length, which makes high-power short-wavelength coherent radiation possible. In a storage ring, due to quantum excitation, the equilibrium longitudinal emittance is mainly the overall contribution of all bend-related elements, such as bends, undulators and laser modulators. By introducing longitudinal Twiss function and analyzing the 6D one-turn map in 3D Twiss form, the longitudinal emittance contribution of all these elements is theoretically studied in this paper, and a general method for minimizing the storage ring equilibrium longitudinal emittance is proposed. An integrated optimization of longitudinal beta function shows, the longitudinal emittance scales as the third power of bending angle, and can be as low as subpicometer with a beam energy of 400 MeV in an ultimate state.

DOI: 10.1103/PhysRevAccelBeams.24.090701

I. INTRODUCTION

Storage ring light sources have become a powerful and irreplaceable tool for scientific researches. Owing to its unique properties such as high brightness, good transverse coherence, excellent polarization and theoretically predictable spectrum, synchrotron radiation widely serves in bioscience, material physics, environmental science and other fields. Until now, the storage ring has experienced three generations, and decades of researches have been carried out on transverse dynamics and emittance optimization. The state-of-the-art fourth-generation storage ring targets at a transverse emittance comparable with that of the produced radiation, or the diffraction limit in other words. Hence these facilities are called diffraction-limited storage ring (DLSR) [1–3]. In or near the soft x-ray range, the corresponding beam transverse emittance is about tens of picometers, and the spectral brightness may reach $10^{23}-10^{24}$ photons s^{-1} mm^{-2} $mrad^{-2}$ $(0.1\%\,\text{bandwidth})^{-1}$ [4]. Physically, such high brightness is actually a result of strong transverse coherence, which is about to be pushed to an ultimate state. Further improvement should concentrate on the longitudinal dimension, i.e., increasing the beam longitudinal coherence.

Similar with the transverse, beam longitudinal coherence depends on the longitudinal emittance, which is much less investigated and optimized in a storage ring. Lower longitudinal emittance means smaller energy spread and shorter bunch; both are of great significance for storage ring based light sources, such as storage ring free-electron laser (SR-FEL) and coherent bend/undulator synchrotron radiation. SR-FEL has long been attractive for the reliable, stable and high-repetition electron beams in the ring [5,6], but the relatively large energy spread suppresses and shifts the microbunching in SASE [7]. A lower energy spread will certainly help to mitigate this effect and reduce the undulator length. In terms of the bunch length, it is well known that the radiated power of a beam at wavelength λ can be expressed as [8]

$$P = N_e P_0[1 + N_e f(\lambda)], \tag{1}$$

with N_e being the electron number of this bunch and P_0 being the radiated power of a single electron. For a Gaussian beam with an rms length of σ_z, $f(\lambda) = \exp[-(\frac{2\pi\sigma_z}{\lambda})^2]$. This factor indicates exactly a strength of longitudinal coherence. Only when the bunch length $\sigma_z \leq \lambda/(2\pi)$, will the coherence be significant. In storage rings, a typical relationship between equilibrium bunch length and energy spread is

*tang.xuh@tsinghua.edu.cn

$\sigma_z = \sqrt{\frac{E_c R_{56}}{eV_0 k \cos\phi_s}}\sigma_\delta$ [9]. E_c, V_0, k, ϕ_s are the standard electron energy, radio frequency (rf) voltage, rf wave number and electron synchrotron phase, respectively. R_{56} is the momentum compaction of the whole ring. To shorten the bunch and produce coherent short-wave radiation, such as terahertz (THz) wave, applying a higher frequency rf system [10] or a lower momentum compaction factor (the "low-alpha" mode) [11,12], helps. However, there exists an ultimate bunch length limit caused by partial alpha effect [13], or more accurately, considering the influence of energy on partial longitudinal phase slippage from radiation emission point to observer, it can be called the partial eta (slip factor) effect [14]. To achieve shorter bunch, apart from low alpha, efforts on low partial eta are also needed, and the lattice must be carefully designed for smaller longitudinal emittance. For instance, in the ten THz range, the required bunch length is on the order of micron, and the partial eta effect will dominate.

On the other hand, steady-state microbunching (SSMB) mechanism has been proposed [15] and actively studied recently [4,14,16–19]. In the case of steady-state coherent THz, as mentioned, low longitudinal emittance is an inevitable requirement. For the future completely laser-driven storage rings, work in Ref. [19] has shown the capability of coherently boosting the radiation as a first step. In the steady state, the diminishment of longitudinal bucket, due to orders of magnitude shorter wavelength when comparing laser and rf, requires a much smaller equilibrium longitudinal emittance. To achieve such a small emittance, however, there is much less experience for the design and optimization of the longitudinal dimension compared with the transverse. Here in this paper, the longitudinal Twiss function is introduced. Thereafter, the three-dimensional Twiss has been all gathered. Then the storage ring one-turn map in 3D Twiss form is deduced, according to which the dispersion, 3D Twiss functions and tune can be directly obtained. We also show that the equilibrium longitudinal emittance can be obtained through an overall integration of longitudinal beta function along the ring. By theoretically analyzing the bend-related elements (bend, undulator, wiggler, laser modulator) and typical arcs, a general method for the optimization of longitudinal beta function is given, and the ultimate state of equilibrium longitudinal emittance of a storage ring is also analyzed in detail.

This paper is organized as the following. In Sec. II, the longitudinal Twiss function is introduced, the full 6×6 one-turn map in 3D Twiss form is deduced, and the calculation method of equilibrium longitudinal emittance is given. Section III analyzes the longitudinal emittance contribution of bend-related elements. Section IV presents the design strategy for ultralow longitudinal emittance, including typical longitudinal-emittance-minimized arcs and the matching of longitudinal Twiss function. Finally, a brief summary is given in Sec. V.

II. LONGITUDINAL BETA FUNCTION AND EQUILIBRIUM EMITTANCE

In accelerator physics, it is convenient and common to use the transfer matrix to describe the linear motion of electrons. Define the horizontal direction being x, and $y(z)$ for the vertical (longitudinal), the linear state of an electron can be expressed by coordinates $X = (x, x', y, y', z, \delta)^T$. Prime terms are a deviation of velocity angles in each transverse plane, and δ is the relative energy deviation. All six coordinates are relative to the designed standard electron, and usually have small values. Electron motion from position A to position B in a lattice can be written as $X_B = M_{A\to B}X_A$, with $M_{A\to B}$ the 6×6 symplectic transfer matrix between these two positions. In particular, when the electron circulates for one turn from A in a storage ring, the map will be $M_{A\to A}$, or M_A for short. For a planar lattice, no skew quadrupoles exist, and there is no coupling between the horizontal and the vertical direction. The 6D symplectic matrix can then be simplified. Since dipoles will naturally introduce transverse and longitudinal coupling in the bending plane, by supposing all dipoles bend electrons horizontally, the transfer map can be reduced to 4×4 for simplicity. Traditionally, to handle the coupling, coordinate x is split into the transverse betatron motion x_β and the contribution of energy deviation $x_\delta = \eta\delta$, where η indicates the dispersion. Then the transverse emittance of one electron, defined as

$$\epsilon_x = \gamma_x x_\beta^2 + 2\alpha_x x_\beta x_\beta' + \beta_x x_\beta'^2, \tag{2}$$

is a constant during movement if radiation is ignored. Here α_x, β_x, γ_x are the horizontal Twiss functions [20].

At a dispersion-free position, including rf, the one-turn map of a ring has the form of

$$M = \begin{pmatrix} \cos\phi_x + \alpha_x \sin\phi_x & \beta_x \sin\phi_x & 0 & 0 \\ -\gamma_x \sin\phi_x & \cos\phi_x - \alpha_x \sin\phi_x & 0 & 0 \\ 0 & 0 & m_{55} & m_{56} \\ 0 & 0 & m_{65} & m_{66} \end{pmatrix},$$

$\phi_x = 2\pi\nu_x$ is the one-turn horizontal betatron phase advance, and ν_x represents the horizontal tune. $e^{\pm i\phi_x}$ are the eigenvalues of top left horizontal 2×2 matrix. Similar with the transverse, for the longitudinal phase space, we can parametrize the bottom right 2×2 matrix as [21]

$$\begin{aligned} m_{55} &= \cos\phi + \alpha \sin\phi, \\ m_{56} &= \beta \sin\phi, \\ m_{65} &= -\gamma \sin\phi, \\ m_{66} &= \cos\phi - \alpha \sin\phi, \end{aligned} \tag{3}$$

with $\phi = 2\pi\nu$ being the one-turn longitudinal synchrotron phase, and ν being the longitudinal tune. $\alpha, \beta, \gamma = \frac{1+\alpha^2}{\beta}$ here stand for the longitudinal Twiss functions. They are of great similarity with their transverse counterparts, except for the magnitude. In most storage rings, the longitudinal focusing is weak, ϕ and α have small values, hence the β and γ keep almost constant, unlike their transverse counterparts.

Generally, most of a ring has dispersion. To analyze the one-turn map of a dispersive position, we focus at an arbitrary place downstream of the above dispersion-free one. The transfer map between is represented as

$$R = \begin{pmatrix} r_{11} & r_{12} & 0 & \eta \\ r_{21} & r_{22} & 0 & \eta' \\ r_{51} & r_{52} & 1 & r_{56} \\ 0 & 0 & 0 & 1 \end{pmatrix}.$$

A symplectic condition implies only six matrix elements are free, the others are correlated through $r_{11}r_{22} - r_{12}r_{21} \equiv 1$, $r_{51} \equiv \eta r_{21} - \eta' r_{11}$ and $r_{52} \equiv \eta r_{22} - \eta' r_{12}$. Here, $r_{56} = -\int_0^{\text{here}} (\frac{\eta(s)}{\rho(s)} - \frac{1}{\gamma_c^2}) ds$ stands for the momentum compaction between these two positions, where γ_c is the Lorentz factor of the standard electron. Then the longitudinal β-function here is obtained by [22]

$$\alpha = \alpha_0 - \gamma_0 r_{56}; \tag{4a}$$

$$\beta = \beta_0 - 2\alpha_0 r_{56} + \gamma_0 r_{56}^2; \tag{4b}$$

$$\gamma = \gamma_0. \tag{4c}$$

In a pure drift section, the γ-function keeps constant, no matter in the transverse or longitudinal dimension. It can only be changed by the focusing elements: quadrupoles in the transverse; rfs or other elements that introduce energy chirp in the longitudinal. The β-function, however, depends quadratically on the drift length: space length L in the transverse and momentum compaction r_{56} in the longitudinal. From this point, r_{56} can be considered as the *longitudinal drift length*. For physical space length, L cannot be negative, while the *longitudinal drift length* can. This brings many differences between these two dimensions. As an example, according to Eqs. (4a) and (4b), the longitudinal β and α have a relation of

$$-\frac{1}{2}\frac{d\beta}{ds} = -\frac{1}{\gamma_0}\alpha\frac{d\alpha}{ds} = \alpha\left[\frac{1}{\gamma_c^2} - \frac{\eta(s)}{\rho(s)}\right].$$

It is quite different from the transverse case by a dispersion related factor $\frac{d\alpha}{ds}$. Because of this factor, the extremums of β locate at either $\alpha = 0$ or $\frac{\eta(s)}{\rho(s)} = \frac{1}{\gamma_c^2}$. In a bend-related element, where $\eta(s)$ and $\rho(s)$ are both nonzero, β can vary much more violently.

In matrix, the one-turn map at this dispersive location can be obtained by $M_x = RMR^{-1}$. Using x_{ij} for matrix elements of M_x, and combining Eqs. (3) and (4), analysis shows that at a dispersive location, the definition of Eq. (3) is also valid, simply replacing m_{ij} by x_{ij} $(j, i = 5, 6)$, except the 56 term. It should be redefined as

$$x_{56} - \mathcal{H}\sin\phi_x = \beta\sin\phi, \tag{5}$$

where $\mathcal{H} = \gamma_x\eta^2 + 2\alpha_x\eta\eta' + \beta_x\eta'^2$ is the chromatic invariant. Thus all the matrix elements are

$$\begin{aligned}
x_{61} &= x_{25} = -\eta'\gamma\sin\phi, \\
x_{62} &= -x_{15} = \eta\gamma\sin\phi, \\
x_{65} &= -\gamma\sin\phi, \\
x_{66} &= m_{66} - r_{56}m_{65} = \cos\phi - \alpha\sin\phi, \\
x_{55} &= m_{55} + r_{56}m_{65} = \cos\phi + \alpha\sin\phi, \\
x_{56} &= m_{56} - (m_{55} - m_{66})r_{56} - m_{65}r_{56}^2 \\
&= \beta\sin\phi + \mathcal{H}\sin\phi_x, \\
x_{11} &= \cos\phi_x + \alpha_x\sin\phi_x - \eta\eta'\gamma\sin\phi, \\
x_{12} &= \beta_x\sin\phi_x + \eta^2\gamma\sin\phi, \\
x_{21} &= -\gamma_x\sin\phi_x - \eta'^2\gamma\sin\phi, \\
x_{22} &= \cos\phi_x - \alpha_x\sin\phi_x + \eta\eta'\gamma\sin\phi, \\
x_{16} &= -\eta(\cos\phi_x + \alpha_x\sin\phi_x) - \eta'\beta_x\sin\phi_x \\
&\quad + \eta(\cos\phi - \alpha\sin\phi), \\
x_{26} &= \eta\gamma_x\sin\phi_x - \eta'(\cos\phi_x - \alpha_x\sin\phi_x) \\
&\quad + \eta'(\cos\phi - \alpha\sin\phi), \\
x_{51} &= -\eta'(\cos\phi_x + \alpha_x\sin\phi_x) - \eta\gamma_x\sin\phi_x \\
&\quad + \eta'(\cos\phi + \alpha\sin\phi), \\
x_{52} &= -\eta'\beta_x\sin\phi_x + \eta(\cos\phi_x - \alpha_x\sin\phi_x) \\
&\quad - \eta(\cos\phi + \alpha\sin\phi).
\end{aligned}$$

This is the general transfer matrix in transverse and longitudinal Twiss function form. Given a one-turn map, both dispersion and Twiss parameters can be quickly deduced. Take dispersion as an example, $\eta = \frac{x_{15}}{x_{65}}$ and $\eta' = \frac{x_{25}}{x_{65}}$.

With the definition of Eqs. (3) and (5), the longitudinal emittance can be defined in a similar way as Eq. (2), with the transverse Twiss functions replaced by their longitudinal counterparts. Just like the transverse, longitudinal emittance ϵ_z of each electron keeps constant if radiation is ignored. Practically, the circulating electrons will give out radiation randomly. When the damping and quantum excitation achieve balance, the beam reaches an

equilibrium state, emittances in three dimensions will hold. To evaluate the steady-state beam properties, Chao's formalism SLIM [23,24] gives the beam distribution second moments at a certain location s as

$$\langle X_i X_j\rangle(s) = 2\sum_{k=x,y,z}\langle|A_k|^2\rangle \mathrm{Re}[E_{ki}(s)E_{ki}^*(s)]. \tag{6}$$

Here, $X_i (i = 1, 2, \ldots, 6)$ is the ith coordinate in X. $E_{ki}(s)$ is the ith element of the eigenvector in the kth dimension. The equilibrium parameter is obtained through

$$\langle|A_k|^2\rangle = C_0\frac{\gamma_c^5}{D_k}\oint\frac{|E_{k5}(\hat{s})|^2}{|\rho(\hat{s})|^3}d\hat{s},$$

where $C_0 = \frac{55}{48\sqrt{3}}\frac{r_e h}{2\pi m_e c}$, m_e, r_e are electron mass and classical radius, respectively. h represents the Planck's constant, D_k is the damping constant of dimension k and $\rho(\hat{s})$ stands for the bending radius at position $\hat{s}$.

Now, we handle Eq. (6) in the planar lattice case. According to the above matrix elements, the eigenvectors of M_{x} are

$$E_x = \begin{pmatrix} -\frac{\eta'\beta_x+(\alpha_x-\mathrm{i})\eta}{\sqrt{2\mathcal{H}}} \\ \frac{\eta\gamma_x+(\alpha_x+\mathrm{i})\eta'}{\sqrt{2\mathcal{H}}} \\ \sqrt{\frac{\mathcal{H}}{2}} \\ 0 \end{pmatrix}, \quad \begin{pmatrix} -\frac{\eta'\beta_x+(\alpha_x+\mathrm{i})\eta}{\sqrt{2\mathcal{H}}} \\ \frac{\eta\gamma_x+(\alpha_x-\mathrm{i})\eta'}{\sqrt{2\mathcal{H}}} \\ \sqrt{\frac{\mathcal{H}}{2}} \\ 0 \end{pmatrix};$$

$$E_z = \begin{pmatrix} \eta\sqrt{\frac{\gamma}{2}} \\ \eta'\sqrt{\frac{\gamma}{2}} \\ \frac{-\alpha+\mathrm{i}}{\sqrt{2\gamma}} \\ \sqrt{\frac{\gamma}{2}} \end{pmatrix}, \quad \begin{pmatrix} \eta\sqrt{\frac{\gamma}{2}} \\ \eta'\sqrt{\frac{\gamma}{2}} \\ \frac{-\alpha-\mathrm{i}}{\sqrt{2\gamma}} \\ \sqrt{\frac{\gamma}{2}} \end{pmatrix}.$$

Substituting these eigenvectors in to Eq. (6), if we define $I_5 = \oint\frac{\mathcal{H}(\hat{s})}{|\rho(\hat{s})|^3}d\hat{s}$ and $I = \oint\frac{\beta(\hat{s})}{|\rho(\hat{s})|^3}d\hat{s}$, one can obtain

$$\langle zz\rangle(s) = \frac{C_0\gamma_c^5}{2}\left[\frac{\mathcal{H}(s)}{D_x}I_5 + \frac{\beta(s)}{D_z}I\right], \tag{7a}$$

$$\langle z\delta\rangle(s) = -\frac{C_0\gamma_c^5}{2}\frac{\alpha(s)}{D_z}I, \tag{7b}$$

$$\langle\delta\delta\rangle(s) = \frac{C_0\gamma_c^5}{2}\frac{\gamma(s)}{D_z}I. \tag{7c}$$

At a dispersion-free location, $\mathcal{H}(s) \equiv 0$. The equilibrium longitudinal emittance has a correlation of $\epsilon_z^2 = \langle zz\rangle\langle\delta\delta\rangle - \langle z\delta\rangle^2$ with the second moments. Hence, the equilibrium longitudinal emittance is

$$\epsilon_z = \frac{C_0\gamma_c^5}{2D_z}I. \tag{8}$$

This form naturally involves the partial eta effect. It applies for a planar lattice and when all rfs are located at dispersion-free locations. In the separated-function-lattice case, the circular integral I can be written as a summation of all elements with $\rho \neq 0$ (bend-related elements). Namely the equilibrium longitudinal emittance can be considered as the contribution of all bend-related elements.

From the expression of second moments [Eqs. (7a) and (7c)], it is clear that the bunch length and energy spread have formulas as

$$\sigma_z = \sqrt{\epsilon_z\beta + \epsilon_x\mathcal{H}}, \tag{9a}$$

$$\sigma_\delta = \sqrt{\epsilon_z\gamma}. \tag{9b}$$

Here, $\epsilon_x = \frac{C_0\gamma_c^5}{2D_x}I_5$ is the equilibrium horizontal emittance. It has the same form as the longitudinal one, Eq. (8). For the horizontal, it is the integration of chromatic invariant that contributes to emittance, but it is the β-function for the longitudinal. From Eq. (9), it is clear that when dispersion is zero, the corresponding bunch length and energy spread have a traditional expression, $\sigma_z = \sqrt{\epsilon_z\beta}$, $\sigma_\delta = \sqrt{\epsilon_z\gamma}$. But more generally, if dispersion shows up, transverse-longitudinal coupling will contribute to bunch length through the $\mathcal{H}$-function [25]. The energy spread, since γ keeps constant until rf appears, is a fixed value between two rfs. For a storage ring with only one rf, the bunch energy spread does not vary along the whole ring.

III. LONGITUDINAL EMITTANCE CONTRIBUTION OF ELEMENTS

In the previous section, the equilibrium longitudinal emittance is obtained by circular integration of the longitudinal β-function, and can be considered as the contribution of all bend-related elements, such as dipoles, undulators (or wigglers) and laser modulators. For each kind of element with length L, define

$$\begin{aligned}\Delta I &= \int_0^L\frac{\beta(\hat{s})}{|\rho(\hat{s})|^3}d\hat{s} \\ &= C_\alpha\alpha_0 + C_\beta\beta_0 + C_\gamma\gamma_0\end{aligned} \tag{10}$$

as the longitudinal emittance contribution coefficient. Here, $(\alpha_0, \beta_0, \gamma_0)$ is the entrance longitudinal Twiss, and C_α, C_β, C_γ are the corresponding coefficients, all being independent of Twiss functions. Considering the relation of γ_0 with α_0 and β_0, ΔI has a minimum value of

$$\Delta I_{\min} = \sqrt{4C_\beta C_\gamma - C_\alpha^2}$$

when $\alpha_0 = -C_\alpha/\Delta I_{\min}$, $\beta_0 = 2C_\gamma/\Delta I_{\min}$ and $\gamma_0 = 2C_\beta/\Delta I_{\min}$. These three Twiss parameters are intrinsic characteristics of the element, and hence called the intrinsic Twiss (IT). For one bend-related element in a ring, if the real entrance longitudinal Twiss matches its IT, the longitudinal emittance contribution of this element is minimized. In this section, we will analyze the longitudinal emittance contribution of typical bend-related elements and the behavior under the IT case.

A. Dipole

Dipole is one of the most common elements for a storage ring. Electrons bend and radiate here, and this means the dipole can also be thought of as a source of damping and quantum excitation. In many rings, the equilibrium longitudinal emittance from the dipole dominates. So we start from the analysis of emittance contribution of a dipole.

According to Eq. (4), for an element, the entrance longitudinal Twiss and the $r_{56}(\hat{\alpha})$ inside determine β together. Assume η_0 and η_0' being the entrance dispersion and dispersion angle of a dipole, and denote the standard electron velocity by β_c, then at an arbitrary bending angle $\hat{\alpha}$ inside the dipole, the accumulated momentum compaction from the entrance can be expressed as [26]

$$r_{56}(\hat{\alpha}) = -\frac{\eta_0 \sin\hat{\alpha}}{\beta_c} - \frac{\eta_0'\rho(1-\cos\hat{\alpha})}{\beta_c} - \frac{\rho(\beta_c^2\hat{\alpha} - \sin\hat{\alpha})}{\beta_c^2}.$$

The longitudinal $\beta(\hat{\alpha})$ function is obtained by substituting this equation into Eq. (4b). Then, setting $\chi = \frac{\eta_0}{\beta_c\rho} - \frac{1}{\beta_c^2}$ and $\kappa = \theta + \frac{\eta_0'}{\beta_c}$, the three coefficients are

$$\begin{aligned}
C_\alpha &= \frac{2\chi}{\rho}(1-\cos\theta) + \frac{\theta^2}{\rho} + \frac{2\eta_0'(\theta - \sin\theta)}{\beta_c\rho},\\
C_\beta &= \frac{\theta}{\rho^2},\\
C_\gamma &= \frac{\eta_0'\chi}{2\beta_c}\cos 2\theta + \frac{\eta_0'^2 - \beta_c^2\chi^2}{4\beta_c^2}\sin 2\theta\\
&\quad + 2\frac{\beta_c\kappa\chi + \eta_0'}{\beta_c}(1-\cos\theta) + 2\frac{\eta_0'\kappa - \beta_c\chi}{\beta_c}(\theta - \sin\theta)\\
&\quad + \frac{\theta^3}{3} - \frac{\eta_0'\theta^2}{\beta_c} - \left(\frac{\eta_0'^2 - \beta_c^2\chi^2}{2\beta_c^2}\right)\theta - \frac{\eta_0'\chi}{2\beta_c}.
\end{aligned} \tag{11}$$

Substituting these coefficients into Eq. (10), the longitudinal emittance contribution of a dipole, ΔI_B, will be obtained. By adjusting the entrance longitudinal Twiss, the motion and radiation property of the electron bunch inside the dipole can be slightly changed, and hence also the contribution to equilibrium longitudinal emittance. Alternatively, it can be seen that the entrance dispersion is also flexible for the minimization of ΔI_B, which may be more convenient and direct sometimes compared with the adjustment of the longitudinal Twiss function.

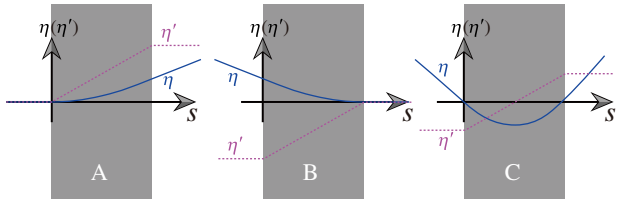

FIG. 1. Three kinds of dipoles based on the entrance dispersion. Each kind has a different contribution to ϵ_z and a different optimization strategy. A: $\eta_0 = \eta_0' = 0$; B: achromatic dipole, $\eta_0 = \rho(1-\cos\theta)/\beta_c$, $\eta_0' = -\tan\theta/\beta_c$; C: general case.

To get a clear understanding of this, the dipoles in a storage ring are classified into three categories based on entrance dispersion, as Fig. 1 shows. The first one (kind A) is usually the first dipole of a super cell. It introduces dispersion downstream, but has an initial dispersion of $\eta_0 = \eta_0' = 0$. This property limits degrees of freedom of emittance optimization. However, it is still very effective by modifying the entrance longitudinal Twiss function, and if IT is matched, the emittance contribution can be reduced in orders. Figure 2 shows the theory limit of ΔI_B. In the condition of high energy and $\gamma_c\theta \gg \sqrt{6}$, $\Delta I_{B\min} \approx \frac{\theta^4}{4\sqrt{7}\rho}$. Adopting a small dipole does help to minimize equilibrium longitudinal emittance. The matched β_0 and α_0 for $\Delta I_{B\min}$ are given in the left part. As the bending angle grows, matched β_0 increases fast, but α_0 varies little. In the small dipole limit or the relative low energy case, β_0 and α_0 also behave similarly. However, when $\gamma_c\theta$ approaches $\sqrt{6}$, violent change occurs because the momentum compaction R_{56} goes to zero. For the achromatic dipole (kind B), its entrance dispersion is also fixed. The theory limit of ΔI_B is exactly that in case A. But the IT β_0 and α_0 vary much since the entrance dispersion is different from that of kind A, as the dashed line shows in the left part of Fig. 2.

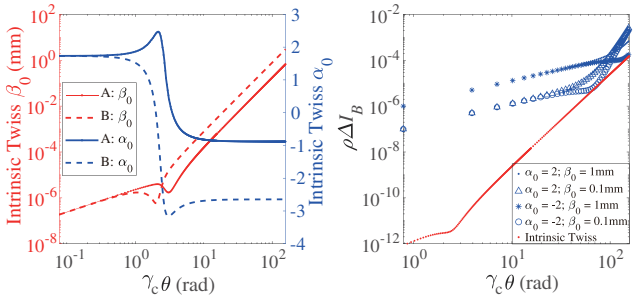

FIG. 2. To minimize the longitudinal emittance contribution of the first two kinds of dipoles (A and B), entrances β_0 and α_0 need to be matched with the IT (left). Both A and B have a same limit of ΔI_B which is shown by the red dotted line in the right figure. Compared with other four cases, in the IT-matched case, ΔI_B can be orders of magnitude smaller. Here, the electron energy is set to be 400 MeV, and the bending radius equals 1 m.

The most general case is the third kind (C), where the initial dispersion provides more space for longitudinal emittance optimization. Concentrating still on the minimum value of ΔI_B, one can find that the initial condition should satisfy

$$\eta_0 = \rho \frac{(1+\beta_c^2)\theta + \beta_c^2 \theta \cos\theta - (1+2\beta_c^2)\sin\theta}{\beta_c(\theta - \sin\theta)}, \tag{12a}$$

$$\eta_0' = -\frac{1}{\beta_c}\tan\frac{\theta}{2}, \tag{12b}$$

$$\alpha_0 \simeq -\sqrt{7}\left(1+\frac{\theta^2}{315}\right), \tag{12c}$$

$$\beta_0 \simeq \frac{\rho\theta^3}{15\sqrt{7}}\left(1+\frac{\theta^2}{60}\right). \tag{12d}$$

Here, throughout this paper, we make a deal that the symbol $\simeq$ is an approximation that is independent of γ_c, but $\approx$ does depend on the standard energy. The first two conditions of these equations indicate that η' at the center of this dipole equals zero, or η has a minimum value [Fig. 3 (left)], which is the condition mentioned in Ref. [27]. The last two indicate the central $\alpha = 0$. However, compared with the dispersion function, the longitudinal beta function inside the dipole undergoes oscillations. The extremums of $\beta(\hat{\alpha})$ come not only from $\alpha = 0$ but also $\frac{\eta}{\rho} = \frac{1}{\gamma_c^2}$. In the optimized case, a proper location of these extremums results in a perfect distribution of β inside, making the partial eta minimized. Hence the longitudinal emittance contribution can be orders of magnitude lower than the unoptimized case, as the black star in Fig. 4 shows.

Applying the above initial condition in Eq. (10), it is safe to conclude that

$$\Delta I_B \simeq \frac{\theta^4}{60\sqrt{7}\rho}\left(1+\frac{\theta^2}{90}\right) \tag{13}$$

when $\theta \leq 0.5$. The longitudinal emittance contribution is proportional to θ^4, as kind A and B dipoles. Figure 5 plots this theory limit. This scaling is very close to the exact result.

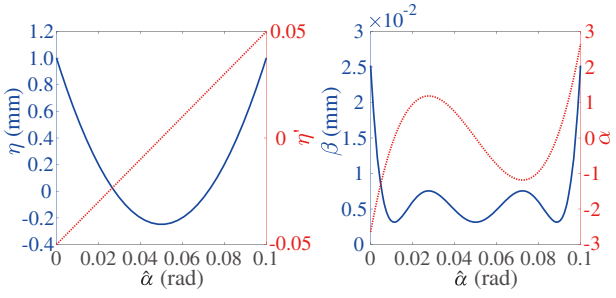

FIG. 3. The matched dispersion (left) and longitudinal Twiss function inside dipole C (right). This distribution minimizes the partial eta effect.

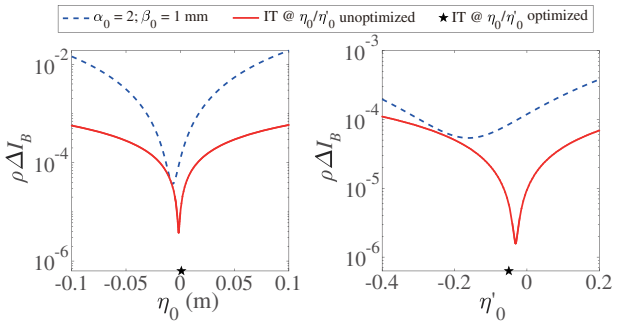

FIG. 4. Longitudinal emittance contribution of the third kind of dipole (C) at various initial dispersions. There exists a minimum in η_0 and η_0' both at a certain entrance Twiss and the IT case. By co-changing η_0, η_0', β_0 and α_0, the longitudinal emittance contribution ΔI_B can be orders of magnitude lower (black star). Here again, the electron energy is set to be 400 MeV, and the bending radius equals 1 m.

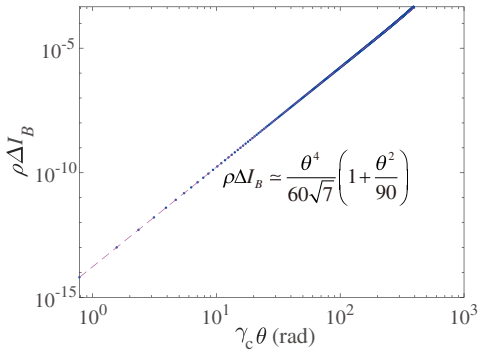

FIG. 5. The theoretic limit of longitudinal emittance contribution of the third kind of dipole (C) at various bending angles. The blue dots are the exact integral results, and the magenta dashed line shows the approximation in the picture, which is valid in a wide range of bending angle.

B. Undulator or wiggler

In addition to dipoles, electrons also radiate in an undulator or wiggler because of the transverse oscillation. This radiation enhances the damping process, changes the damping partition, and results in a smaller equilibrium transverse emittance [28]. Owing to this property, damping wigglers are widely used in the third-generation storage rings, and are almost indispensable for DLSRs. Apart from the transverse effect, the radiation will also affect the longitudinal emittance.

Consider an ideal planar undulator or wiggler. The magnetic field on the central plane can be written as

$$B(z) = B_0 \cos(k_u z),$$

with B_0 representing the peak magnetic field and $k_u = \frac{2\pi}{\lambda_u}$. Under such a field, a relativistic electron will oscillate transversely when passing through. During this process, the motion angle is

$$x' = \frac{v_x}{v_z} = \frac{K}{\gamma_c}\sin(k_u z).$$

Here, $K = \frac{eB_0}{m_e c k_u}$ is the dimensionless strength of the undulator. It can be proven that the derivative of the dispersion function inside, $\eta'(z)$, also has the same form, hence the dispersion

$$\eta(z) = \int_0^z \eta'(\tilde{z})ds = \eta_0 + \frac{K}{\gamma_c k_u}[1 - \cos(k_u z)], \quad (14)$$

where the typical case $\gamma_c \gg K$ is assumed, and the infinitesimal $ds = \sqrt{1 + x'^2}d\tilde{z} \approx (1 + \frac{x'^2}{2})d\tilde{z}$ is used. η_0 represents the entrance dispersion of this undulator. A nonzero η_0 indicates that the undulator is placed at a dispersive section.

The calculation of longitudinal emittance contribution relies on the exact internal momentum compaction factor. Considering the resonant condition $\lambda = \frac{\lambda_u}{2\gamma_c^2}(1 + \frac{K^2}{2})$, longitudinal dispersive strength inside can be expressed as

$$\begin{aligned} r_{56}(z) &= \int_0^z \left(-\frac{\eta(\tilde{z})}{\rho(\tilde{z})} + \frac{1}{\gamma_c^2}\right)\left(1 + \frac{x'^2}{2}\right)d\tilde{z} \\ &\approx \frac{2\lambda z}{\lambda_u} - \frac{K^2\,\sin(k_u z)}{\gamma_c^2 k_u}\left[1 + \frac{\gamma_c k_u \eta_0}{K} - \frac{\cos(k_u z)}{2}\right]. \end{aligned} \quad (15)$$

At the exit, $z \equiv L_u$, and $\sin(k_u L_u) \equiv 0$. This means a total undulator momentum compaction of

$$r_{56}^u = \frac{2\lambda L u}{\lambda_u} = 2N_u\lambda = \frac{L_u}{\gamma_c^2}\left(1 + \frac{K^2}{2}\right). \quad (16)$$

Here, N_u represents the number of undulator periods. This formula indicates that the r_{56} of each period is just two times of the fundamental resonant radiation wavelength, λ, no matter if the undulator is placed dispersively or not.

Again, by assuming α_0, β_0 and γ_0 being the entrance Twiss, the longitudinal beta inside $\beta(z)$ can be obtained through Eqs. (4b) and (15). In the undulator, the sine term of $r_{56}(z)$ leads to an oscillation in β-function. In the low longitudinal emittance case, this is a vital point for partial eta effect, similar with that of the whole ring. Therefore, the contributed longitudinal emittance by an undulator period is $\Delta\epsilon_{zi} = C_0\frac{\gamma_c^5}{2\alpha_z}\Delta I_i$, and

$$\begin{aligned} \Delta I_i &= \int_0^{\lambda_u} \frac{\beta(z)}{|\rho^3(z)|}\left(1 + \frac{x'^2}{2}\right)dz \\ &= C(\alpha_i, \beta_i, \gamma_i)^T, \end{aligned} \quad (17)$$

where $(\alpha_i, \beta_i, \gamma_i)^T$ is the entrance longitudinal Twiss of this period, $C = (C_\alpha, C_\beta, C_\gamma)$, and for undulator or wiggler

$$\begin{aligned} C_\alpha &= -\frac{16K^3k_u^2\lambda}{3\gamma_c^3}; \\ C_\beta &= \frac{8K^3k_u^2}{3\gamma_c^3}; \\ C_\gamma &= -\frac{K^3}{\gamma_c^7}\left(\frac{160}{27} + \frac{3712K^2}{675} + \frac{3112K^4}{4725}\right) \\ &\quad + \frac{\pi K^3}{\gamma_c^7}\left(\frac{28}{9} + \frac{167K^2}{45} + \frac{97K^4}{90}\right) \\ &\quad + \frac{10\pi^2K^3}{3\gamma_c^7}\left(1 + \frac{K^2}{2}\right)^2. \end{aligned} \quad (18)$$

The three parameters depend strongly on the energy of the standard electron. But for a given undulator and beam energy, they are all constants. Looking closely at the three terms $\alpha_i C_\alpha$, $\beta_i C_\beta$ and $\gamma_i C_\gamma$, we have known that γ_i keeps constant inside the undulator since no rf kick exists. Therefore, for each undulator period, the variation of emittance contribution, ΔI_i, comes only from the first two terms, α_i and β_i more specifically.

For each undulator period, $(\alpha_i, \beta_i, \gamma_i)^T$ is connected with each other by the longitudinal transfer map in between. We have analyzed previously that each period has a momentum compaction of 2λ, this corresponds to a Twiss function transfer map:

$$T_D = \begin{pmatrix} 1 & 0 & -2\lambda \\ -4\lambda & 1 & 4\lambda^2 \\ 0 & 0 & 1 \end{pmatrix}.$$

Because the initial Twiss value at the entrance of the undulator is $(\alpha_0, \beta_0, \gamma_0)$, at the entrance of the ith undulator period, by iteration, $(\alpha_i, \beta_i, \gamma_i)^T = T_D^{i-1}(\alpha_0, \beta_0, \gamma_0)^T$. Inside the undulator, α_i depends linearly on z, while β_i depends quadratically. Applying this value to each period, the contribution coefficient ΔI_i is obtained. The total longitudinal emittance contribution coefficient by the whole undulator is the summation of all periods, hence can be written into

$$\begin{aligned} \Delta I_u &= \sum_{i=0}^{N_u-1}\Delta I_i = C\left(\sum_{i=0}^{N_u-1} T_D^i\right)(\alpha_0, \beta_0, \gamma_0)^T \\ &= N_u C\begin{pmatrix} 1 & 0 & (1-N_u)\lambda \\ 2(1-N_u)\lambda & 1 & \frac{2(N_u-1)(2N_u-1)}{3}\lambda^2 \\ 0 & 0 & 1 \end{pmatrix}\begin{pmatrix} \alpha_0 \\ \beta_0 \\ \gamma_0 \end{pmatrix}. \end{aligned} \quad (19)$$

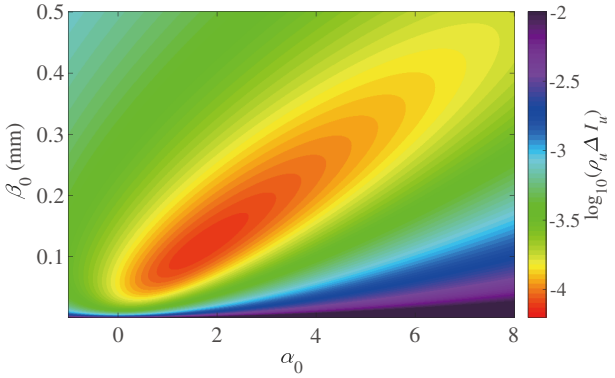

FIG. 6. The contribution coefficient ΔI_u to the longitudinal emittance of an undulator or wiggler. To make it dimensionless, the peak curvature radius of the undulator $\rho_u = \frac{\gamma_c}{K k_u}$ is multiplied. The wiggler parameters are $\lambda_U = 5$ cm, $N_u = 50$, and $K = 6.857$. The best value appears around $(\alpha_0, \beta_0) = (1.64, 112\ \mu\text{m})$.

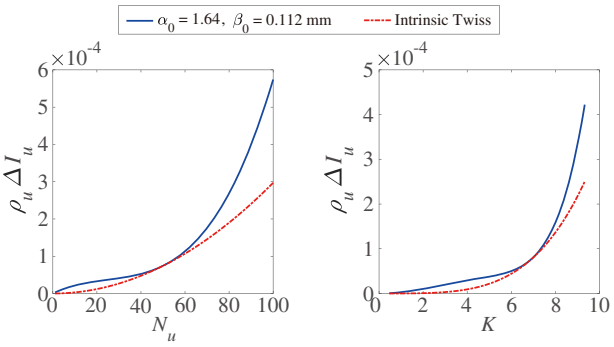

FIG. 7. The contribution coefficient ΔI_u to longitudinal emittance of an undulator or wiggler vs N_u (left) and K (right). To make it dimensionless, the peak curvature radius of the undulator ρ_u is multiplied. The blue solid line is the result at $(\alpha_0, \beta_0) = (1.64, 112\ \mu\text{m})$. For each N_u and K, there exists an optimized α_0 and β_0, red dashed line gives the optimized result. Here, $\lambda_U = 5$ cm, $K = 6.857$.

It is clear that for an undulator or wiggler, its longitudinal emittance contribution depends linearly on initial Twiss parameters, α_0, β_0 and γ_0. However, if the relationship $\gamma_0 = \frac{1+\alpha_0^2}{\beta_0}$ is considered, there will be an optimized value. Figure 6 shows the emittance contribution $\rho_u \Delta I_u$ under various initial α_0 and β_0. When the initial beta is small while gradient (α_0) is large, this contribution is significant. But if optimized, several orders of magnitude reduction can be obtained. The best initial condition satisfies that the central α equals zero, namely β at the undulator center reaches a minimum value. Under such a circumstance, the variation of equilibrium bunch length along the undulator is minimized, so is the emittance contribution.

From Eq. (19), undulator period number N_u or length contributes much more linearly to emittance growth than initial Twiss. When N_u increases, the beam transit time linearly enhances, which is the reason of the first linear N_u term. The N_u in the 3×3 matrix comes from the fact that the beam longitudinal state, or $\beta(z)$, varies along the undulator, and this causes extra contribution. To get a clearer understanding about the influence of N_u, we set $(\alpha_0, \beta_0) = (1.64, 112\ \mu\text{m})$, calculate and plot the longitudinal emittance contribution coefficient as the blue solid line in the left of Fig. 7. As undulator period number increases, ΔI_u grows fast, especially in the large N_u range. But this can be suppressed by optimizing α_0 and β_0 for each case of period number [Fig. 7 (left, red dashed line)]. If this is done, the contribution coefficient,

$$\Delta I_u = \frac{N_u}{3}\sqrt{-9C_\alpha^2 + 36C_\beta C_\gamma + 12C_\beta^2(N_u^2 - 1)\lambda^2},$$

depends quadratically on N_u. At the large N_u case, the emittance contribution can be greatly reduced.

Practically, a more common situation is to adjust the undulator gap to modify the K parameter. During this operation, only undulator period length keeps unchanged, while the other parameters will be modified. Compared with the dependence on N_u, the longitudinal emittance contribution is much more sensitive to K. For the fixed-initial-Twiss case, as given by the blue solid line in the right of Fig. 7, at large K range, ΔI_u is beyond the fifth order of K. If optimized, $\Delta I_u \sim 4.8369 k_u N_u^2 K^5/\gamma_c^5$ when $K \gg 1$, and $\Delta I_u \sim 9.6736 k_u N_u^2 K^3/\gamma_c^5$ when $K \ll 1$, as presented by the red dashed line in the right of Fig. 7.

If the undulator or wiggler locates at a dispersive position, say $\eta_0 \neq 0$ and $\eta_0' = 0$, there will be an extra contribution to longitudinal emittance. Substituting Eq. (15) into Eq. (17), one can find that only C_γ is changed. Two new terms that are related with η_0, $\frac{8K^5 k_u^2 \eta_0^2}{15\gamma_c^5}$ and $\frac{K^4 k_u[30\pi + K^2(32+15\pi)]\eta_0}{30\gamma_c^6}$, need to be added to the dispersionless case. Hence the total longitudinal emittance contribution becomes

$$\begin{aligned}\Delta I_u &= \Delta I_{u,\text{nodis}} + \Delta I_{u,\text{dis}} \\ &= \Delta I_{u,\text{nodis}} + \frac{8K^5 k_u^2 \eta_0^2}{15\gamma_c^5}\gamma_0 \\ &\quad + \frac{K^4 k_u[30\pi + K^2(32+15\pi)]\eta_0}{30\gamma_c^6}\gamma_0, \end{aligned} \tag{20}$$

which is quadratically dependent on initial dispersion. Figure 8 presents the influence of η_0. To minimize the total emittance contribution, one can put the undulator or wiggler at a position with a small negative dispersion. But this does not help much compared with the dispersionless case, and may introduce other transverse problems, such as extra transverse emittance increment.

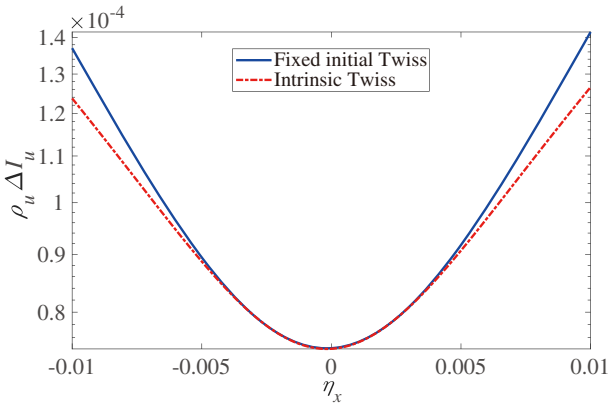

FIG. 8. The contribution coefficient ΔI_u to longitudinal emittance when the undulator or wiggler is located at a dispersive position. The blue solid line is the result at $(\alpha_0, \beta_0) = (1.64, 114\ \mu\text{m})$. For each η_0, there exists an optimized α_0 and β_0, and the red dashed line gives the optimized result. $\lambda_U = 5$ cm, $N_u = 50$.

C. Laser modulator

As electrons passing through a planar wiggler or undulator, if a laser, with wavelength matched at the resonant condition $\lambda = \frac{\lambda_u}{2\gamma_c^2}(1 + \frac{K^2}{2})$, joins in, its electric field will interact continuously with the electrons' transverse velocity, and energy exchange will occur between the electron and laser. Depending on the initial phase of the electron as entering the wiggler or undulator, the energy gain can either be positive or negative. This effect has been extensively studied in both FEL and inverse free-electron laser [29,30]. When the wiggler or undulator is ideal and is put in a dispersion-free section, the whole interaction process makes no difference to beam transverse property, and is hence a 1D dynamic problem. The beam dynamics can be described by the famous FEL pendulum equation:

$$\frac{d\delta}{dz} = \frac{ka_0KJ}{2\gamma_c^2}\sin\hat{\phi}, \tag{21a}$$

$$\frac{d\hat{\phi}}{dz} = 2k_u\delta. \tag{21b}$$

Here, $k = \frac{2\pi}{\lambda}$ is the laser wave number, $a_0 = \frac{eE_0}{m_e kc^2}$ is the dimensionless laser electric field strength, and $J = J_0(\frac{K^2}{4+2K^2}) - J_1(\frac{K^2}{4+2K^2})$ is a Bessel factor. $\hat{\phi} = (k + k_u)z - kct + \hat{\phi}_0$ is the ponderomotive phase. Figure 9 shows the final longitudinal phase space of a line bunch after passing through the combined fields.

Typically, it can be seen that for a standard electron (initial phase $\hat{\phi}_0 = 0$, also the zero-cross point of each subfigure), its energy does not change after passing through the laser modulator. Electrons at other phases are accelerated or decelerated. In other words, the whole bunch is

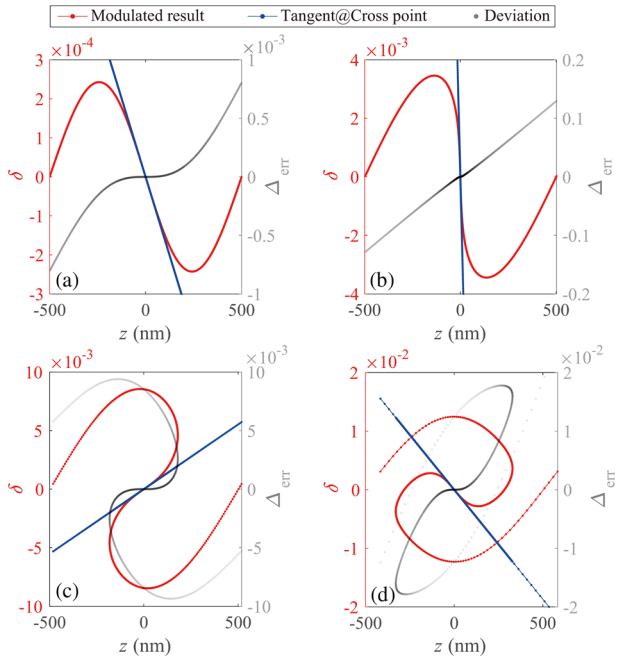

FIG. 9. Longitudinal phase space at the exit of the laser modulator under various laser strength. The initial state is a line bunch without energy deviation. As the modulation laser strength grows, electrons rotate and form the FEL bucket, but the linear region around the zero-cross point shrinks. The blue dotted line is the tangent at the zero-cross point, the gray dotted line represents the deviation between modulated result and the linear tangent line. (a) $a_0 = 3.9 \times 10^{-6}$; (b) $a_0 = 5.8 \times 10^{-5}$; (c) $a_0 = 1.9 \times 10^{-4}$; (d) $a_0 = 3.9 \times 10^{-4}$. The laser wavelength used is $\lambda = 1\ \mu$m, which is the fundamental resonant wavelength of the undulator with $\lambda_u = 5$ cm, and wiggler periods $N_u = 50$.

modulated. When the laser is weak, the modulation approaches a sinusoidal or cosinoidal form. But for a strong laser, the modulation inside the wiggler will cause a large energy change during every wiggler period. Then, electrons with positive δ slip forward and negative backward, resulting in a significant longitudinal phase space rotation around $2(n+1)\pi$. If the laser is strong or the wiggler period number is large, this period-by-period effect will finally lead to a phase space rotation in an FEL bucket. The linear region, which is around the standard electron and the most frequently concerned, will shrink as the phase space rotation angle increases.

Despite the complexity, the modulation property is very suitable for the replacement of rfs in a storage ring, pushing the modulation wavelength from tens of centimeters to micron, and promoting bunches to microbunches [14]. However, before more detailed analyses, we should make it clear that there are at least two issues that are very different from a thin-lens rf. The first one is the longitudinal transfer matrix; the second is that the laser modulator will contribute to equilibrium longitudinal emittance.

We have stated that if the laser modulator is located somewhere dispersionless, the averaged longitudinal

motion of the electron can be described by Eq. (21). To get the symplectic transfer matrix, we consider those electrons close to the standard one ($\hat{\phi}$ is small), and linearize Eq. (21a) as

$$\frac{d\delta}{dz} = \frac{ka_0 K J}{2\gamma_c^2}\cos\phi_s \cdot \hat{\phi}.$$

Here, for a more general case, we assume that the standard electron has a phase of ϕ_s. Thus, the motion in the combined fields can be written into

$$\begin{pmatrix} z \\ \delta \end{pmatrix} = \begin{pmatrix} \cos\Delta\psi_m & \frac{2\sin\Delta\psi_m}{\nu_m k} \\ -\frac{\nu_m k \sin\Delta\psi_m}{2} & \cos\Delta\psi_m \end{pmatrix} \begin{pmatrix} z_0 \\ \delta_0 \end{pmatrix}, \quad (22)$$

and $\nu_m = \sqrt{-\frac{4a_0 KJ}{2+K^2}\cos\phi_s}$, $\Delta\psi_m = N_u\Delta\psi_1 = 2\pi N_u\nu_m$ is the equivalent longitudinal Twiss phase advance in N_u periods. This is the transfer map of the laser modulator in a thick-lens model. Setting $N_u = 1$, the single period map is

$$M_{m,1} = \begin{pmatrix} 1 & 0 \\ h & 1 \end{pmatrix}\begin{pmatrix} 1 & \frac{2\sin\Delta\psi_1}{\nu_m k} \\ 0 & 1 \end{pmatrix}\begin{pmatrix} 1 & 0 \\ h & 1 \end{pmatrix}. \quad (23)$$

Here, $h = -\frac{\nu_m k \tan(\pi\nu_m)}{2}$ is a small energy kick strength and $\frac{2\sin\Delta\psi_1}{\nu_m k}$ is the equivalent *longitudinal drift strength*. When $2\pi\nu_m \ll 1$, $\frac{2\sin\Delta\psi_1}{\nu_m k} \approx 2\lambda$. This exactly indicates an r_{56} of 2λ per undulator period, and the single period modulation map is the result of one *longitudinal drift* map sandwiched by two energy kicks. It should be noted that for a laser modulator, to get enough modulation, the wiggler usually has a large K, hence the above approximation is valid when $a_0 \ll 0.01$.

For the longitudinal emittance contribution of a laser modulator, Eq. (23) has given a clear clue for the handling method. The overriding difference between a laser modulator and a pure wiggler or undulator (or laser is off) is that the former has energy kicks inside. These energy kicks change the longitudinal β-function from the laser-off case. This variation in β affects the equilibrium longitudinal emittance contribution. By putting two small energy kicks at the head and tail of each wiggler period, and following the method in the undulator case, the corresponding Twiss transfer map of Eq. (23) is then

$$T_M = \begin{pmatrix} \cos(2\Delta\psi_1) & \frac{\nu_m k\sin(2\Delta\psi_1)}{4} & -\frac{\sin(2\Delta\psi_1)}{\nu_m k} \\ -\frac{2\sin(2\Delta\psi_1)}{\nu_m k} & \cos^2\Delta\psi_1 & \frac{4\sin^2\Delta\psi_1}{\nu_m^2 k^2} \\ \frac{\nu_m k\sin(2\Delta\psi_1)}{4} & \frac{1}{4}\nu_m^2 k^2\sin^2\Delta\psi_1 & \cos^2\Delta\psi_1 \end{pmatrix}.$$

However, this transfer map does not bring the Twiss function to the real front of the next period dipole, since there exists one more energy kick, and the corresponding map is

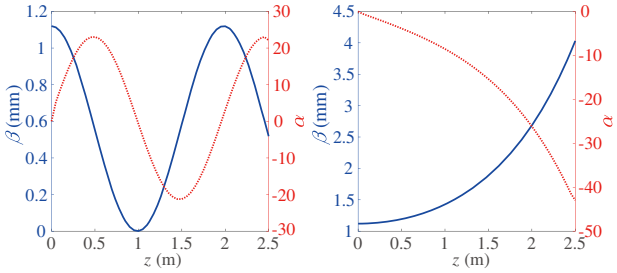

FIG. 10. Longitudinal Twiss function inside a laser modulator at different synchrotron phases. Left: $\phi_s = \pi$ and $a_0 = 4\times10^{-4}$, Twiss function oscillates. Right: $\phi_s = 0$ and $a_0 = 4\times10^{-5}$, Twiss function diverges.

$$T_K = \begin{pmatrix} 1 & -h & 0 \\ 0 & 1 & 0 \\ -2h & h^2 & 1 \end{pmatrix}.$$

Therefore, the entrance Twiss of the ith laser modulator period will be $(\alpha_i,\beta_i,\gamma_i)^T = T_K T_M^{i-1}(\alpha_0,\beta_0,\gamma_0)^T$. Figure 10 presents the longitudinal Twiss function inside a laser modulator under different synchronous phases. When ϕ_s is around π, both α and β oscillate sinusoidally or cosinoidally, and the oscillation wavelength is $\frac{\lambda_u}{2\nu_m}$, which reduces as the laser strength increases. The central and peak-to-peak values of β are $\beta_{\rm cen} = \frac{\beta_0}{2} + \frac{2\gamma_0}{k^2\nu_m^2}$ and $\Delta\beta_{\rm pp} = \frac{4}{k^2\nu_m^2\beta_{\rm cen}}$. At small a_0, the second term of $\beta_{\rm cen}$ may contribute significantly. A large $\beta_{\rm cen}$ means a large equilibrium longitudinal emittance contribution. In another case, if the synchrotron phase is around zero, which indicates ν_m is an imaginary number, the Twiss inside modulator diverges, as the right of Fig. 10 shows. This would result in vast increasing of β, and hence a much larger longitudinal emittance contribution.

It should be stated that the above discussion of longitudinal beta is only the averaged performance; a more

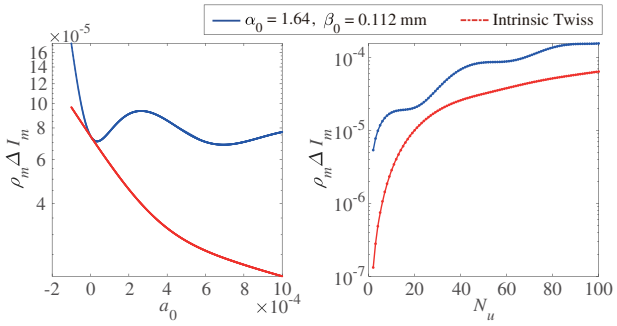

FIG. 11. Longitudinal emittance contribution of a laser modulator under various laser strength (left) and undulator period numbers (right). In the left part, modulator period number is fixed at 50, $\lambda_u = 5$ cm. Negative a_0 means a zero synchrotron phase, and $a_0 > 0$ for $\phi_s = \pi$. In the right part, a_0 is tuned at 4×10^{-4}. ρ_m is the peak bending radius of the laser modulator.

sophisticated evolution exists in every period because of a constantly changing bending radius and energy kick. To embrace these effects, analytically, eigenvectors and eigenvalues of $T_K T_M^{i-1}$ can be used to obtain the total longitudinal emittance contribution coefficient by the laser modulator, which finally can be written as

$$\Delta I_m = CT_K\left(\sum_{i=0}^{N_u-1} T_M^i\right)(\alpha_0,\beta_0,\gamma_0)^T = \frac{C}{\sin\Delta\psi_1}\begin{pmatrix} \frac{\cos\frac{\tilde{\Delta}}{2}\sin(\Delta\psi_m)}{\cos\frac{\Delta\psi_1}{2}} & -\frac{\nu_m k(N_u\sin\frac{\Delta\psi_1}{2}\sin\Delta\psi_1+\sin\frac{\tilde{\Delta}}{2}\sin\Delta\psi_m)}{4\cos\frac{\Delta\psi_1}{2}} & \frac{N_u\sin\frac{\Delta\psi_1}{2}\sin\Delta\psi_1-\sin\frac{\tilde{\Delta}}{2}\sin\Delta\psi_m}{\nu_m k\cos\frac{\Delta\psi_1}{2}} \\ -\frac{\cos\Delta\psi_1-\cos\tilde{\Delta}}{\nu_m k} & \frac{(1+2N_u)\sin\Delta\psi_1+\sin\tilde{\Delta}}{4} & -\frac{(1-2N_u)\sin\Delta\psi_1+\sin\tilde{\Delta}}{\nu_m^2k^2} \\ \frac{\nu_m k\sin^2\Delta\psi_m}{2\cos^2\frac{\Delta\psi_1}{2}} & \frac{\nu_m^2k^2(2N_u\sin\Delta\psi_1-\sin 2\Delta\psi_m)}{16\cos^2\frac{\Delta\psi_1}{2}} & \frac{2N_u\sin\Delta\psi_1+\sin 2\Delta\psi_m}{4\cos^2\frac{\Delta\psi_1}{2}} \end{pmatrix}\begin{pmatrix}\alpha_0\\ \beta_0\\ \gamma_0\end{pmatrix}. \quad (24)$$

Here, $\tilde{\Delta} = (2N_u - 1)2\pi\nu_m$. According to this expression, the dependence on laser strength is analyzed, shown in the left part of Fig. 11. Generally, when the entrance β_0 deviates far from the optimized value, ΔI_m has a small oscillation as the laser strength improves. This indicates a series of a_0 which make the emittance contribution minimum. However, when β_0 approaches the optimization, the oscillation vanishes gradually. Finally, at the best initial state, ΔI_m drops monotonously with the growth of a_0 and can be greatly reduced by increasing laser strength. Besides, the influence of modulator period number is also analyzed as the right of Fig. 11 presents. The stepwise growth is a typical case, which originates from the sinusoidal nature of the β-function. At the best state, like the dependence on laser, the stepwise property vanishes again.

IV. ULTRALOW LONGITUDINAL EMITTANCE STORAGE RINGS

In the previous section, several typical bend-related elements are analyzed on their equilibrium longitudinal emittance contribution and longitudinal Twiss functions evolution. In this section, the matching of longitudinal Twiss functions, like the transverse ones, is discussed. Based on the above results, the limit state of longitudinal emittance of some typical arcs and a storage ring is analyzed. Two samples of storage ring targeting at ultralow longitudinal emittance are presented. Of course, to keep the flexibility in the transverse, only the longitudinal profile is given.

A. Longitudinal drift section

In the transverse direction, one drift section is a real empty space. But for the longitudinal, one drift is an achromatic section, namely a beam line that has only the momentum compaction effect (r_{56}). Figure 12 shows three kinds of typical longitudinal drift sections. The simplest one is of course a real empty space. By changing the space length L, the r_{56} alters. But for high energy particles, a significant value of r_{56} means a huge length. A clever design is the magnetic chicane, where the longitudinal drift can be tuned without increasing or decreasing the real space length, adjusting the dipole bending angle instead. This greatly reduces the beam line length, especially for relativistic particles. The third kind is an arc, where the entrance and exit direction of beam can be different. Double-bend achromat (DBA), triple-bend achromat (TBA) and multi-bend achromat (MBA) are all typical longitudinal drift sections. In these cases, achromatic condition requires that the first and last dipoles must have a fixed boundary, hence the r_{56} from the two bends cannot be changed. Thus, for DBA, the r_{56} can only be modified by varying space length in between or changing the bending angle. To adjust r_{56} more conveniently, one (TBA) or more (MBA) dipoles can be added in between. Unlike the chicane, the adjustment of longitudinal drift depends on tuning of quadrupole strength which causes a modification of dispersion inside the added dipoles. Although the introduction of dipoles breaks the space limitation for a significant r_{56}, they may bring large high order momentum compaction if not carefully controlled. Besides, as previously introduced, these dipoles will contribute to the longitudinal emittance due to radiation, and this needs to be minimized when low energy spread or ultrashort bunch is needed.

B. Ultimate-longitudinal-emittance arcs

It is clear that in an arc, the longitudinal emittance limitation appears when and only when every dipole has a

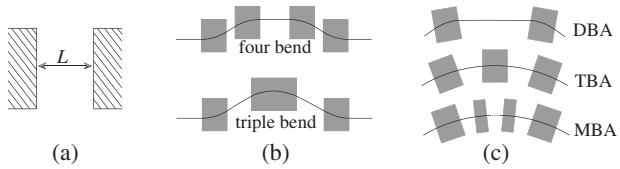

FIG. 12. Three kinds of typical longitudinal drift section. (a) Pure empty space, $r_{56} = \frac{L}{\beta_c^2\gamma_c^2}$. (b) Four-bend and triple-bend chicane. (c) A series arcs: DBA, TBA, MBA.

theoretic minimum emittance contribution. This indicates a same IT γ for all three kinds of dipoles A, B and C.

Because dipoles in kind A and kind B are usually used to match the dispersion, from now on, we take θ_m and ρ_m as their bending angle and bending radius, respectively. The subscript m here represents *matching*. For these two kinds of dipoles, from Eq. (11), if they have the same bending angle and radius, the IT γ for both are consistent naturally. In a common case, when $\gamma_c\theta_m \gg 1$, it is safe to write it as

$$\gamma_m \approx \frac{8\sqrt{7}\beta_c^2}{\theta_m^3\rho_m}.$$

In a DBA, the separation between two dipoles can be optimized to make them both work at the emittance-minimized state. This separation is

$$L_s = \rho_m\gamma_c^2\frac{2-2\cos\theta_m+\beta_c^2\theta_m^2-2\theta_m\sin\theta_m}{\theta_m} \approx \frac{\gamma_c^2\rho_m\theta_m^3}{4}. \tag{25}$$

Figure 13(a) shows an example of matched longitudinal Twiss in DBA. The longitudinal β-function varies quadratically in separated space, and matches the optimized longitudinal Twiss of two dipoles.

The dipole in kind C is a general case, and is widely used in a storage ring supercell. We call it the main dipole.

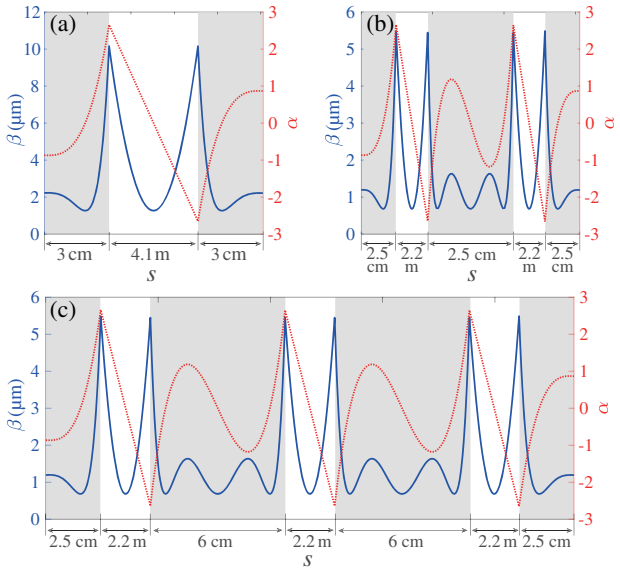

FIG. 13. Matched longitudinal Twiss of three typical arcs. The Twiss functions inside every dipole are their IT. (a) DBA; (b) TBA; (c) MBA. The x-axis represents the longitudinal position along this section. To show the details inside the dipole (with gray background), the location of the dipole is zoomed in and adopts a unit of centimeter. For the separation between dipoles (without background), where β changes quadratically, the x-axis unit is meter. In each element, the scale of the x-axis is linear.

Previously we have analyzed the best initial longitudinal Twiss for minimum emittance contribution, which is

$$\gamma \simeq \frac{120\sqrt{7}}{\rho\theta^3}.$$

When main dipoles and match dipoles both exist in a beam line, like TBA and MBA, the minimum longitudinal emittance state requires $\gamma = \gamma_m$. This means a bending angle relation between the main dipole and match dipole of $\beta_c^2\rho\theta^3 = 15\rho_m\theta_m^3$. Another condition is the matching of the longitudinal β-function. Similar with the DBA bends, a separation with length

$$L_{mc} \approx \frac{\gamma_c^2\rho_m\theta_m^3}{4} \tag{26}$$

will be the perfect choice for the matching of the main and achromatic dipoles. Figure 13(b) presents a matched TBA case. The longitudinal β-function varies violently inside the dipole, but can be perfectly transformed between them through an empty space. Actually, more dipoles can be added and form MBA structure, with each dipole working in an emittance-minimized state. Assuming all main dipoles are the same, then the matching of the β-function between main dipoles can also be accomplished by a separation. From Eqs. (12c) and (12d), the space equals

$$L_c = \frac{\beta_c^2\gamma_c^2\rho(\theta^2+\theta\ \sin\ \theta-4+4\ \cos\ \theta)}{\theta-\sin\ \theta} \approx \frac{\beta_c^2\gamma_c^2\rho\theta^3}{60}. \tag{27}$$

Just like L_{mc}, L_c is also proportional to θ^3. Put arbitrary numbers of main dipoles in DBA, and separate each other by this length, with L_{mc} between match and main dipoles, one longitudinal-emittance-minimized MBA can be formed. Figure 13(c) is an example of a Twiss function of a four-bend achromat.

C. Ultimate-longitudinal-emittance storage ring

In a storage ring, to achieve an ultimate-longitudinal-emittance state, the arcs introduced previously can be used. However, to form a ring, one more constraint about the bending angle exists. Assuming the ring consists of N_s arcs. Each arc has two match bends and N_c main dipoles. The constraint reads $N_s(2\theta_m + N_c\theta) = 2\pi$. Besides, to make the beam stable, the matching of the longitudinal Twiss function between theses arcs is needed. Typically, this matching can be accomplished in two ways.

The first one, similar with the transformation of a longitudinal Twiss inside arcs, depends on a pure empty space. It can be seen that when the separation is

$$L_d = \gamma_c^2 \rho_m \frac{-2 + 2\cos\theta_m + \beta_c^2 \theta_m^2}{\theta_m} \approx \gamma_c^2 \rho_m \left(-\frac{\theta_m}{\gamma_c^2} + \frac{\theta_m^3}{12} - \frac{\theta_m^5}{360} \right), \quad (28)$$

the longitudinal β-function of two arcs will be perfectly connected. In other words, the combination of this separation and an arc forms a completely isochronous longitudinal supercell.

The other way takes advantage of the longitudinal focusing property of an rf or laser modulator to match the longitudinal β. If only one rf or laser modulator is used for matching, it must be set at the separation center. In thin lens approximation, its modulation strength must satisfy

$$h = \frac{eV_0}{E_c} k = \frac{2(\alpha_0 - \gamma_0 \xi)}{-2\alpha_0 \xi + \beta_0 + \gamma_0 \xi^2},$$

where $\xi = \frac{L_{mrf}}{\gamma_c^2}$. L_{mrf} is the separation between the rf or modulator and the nearby matching dipole, and $(\alpha_0, \beta_0, \gamma_0)$ represents the boundary longitudinal Twiss of the emittance-minimized state. When this matching is completed, the longitudinal stability is naturally fulfilled. Figure 14(a) shows an example of this circumstance. If $2L_{mrf} < L_d$, r_{56} of the whole ring is negative, and $h > 0$; vice versa. The further $2L_{mrf}$ deviates from L_d, the stronger the required modulation strength will be. In the case that $L_{mrf} > L_d$, both α and β at the position of rf or laser modulator will have a large value [as Fig. 14(a) shows], which means a rather long bunch, and a serious nonlinear effect from rf or laser modulator. An alternative choice is to apply two rfs or laser modulators which are set symmetrically, as shown by Fig. 14(b). There is little requirement on the modulation strength in this case. From the point of longitudinal Twiss matching, only physical separations and dipoles can form periodic Twiss structures, and it seems that the electrons will be stable in such a ring. But from the point of energy conservation, rfs or laser modulators are necessary to compensate the radiation loss. Obviously, there should be at least one rf or laser modulator in a ring.

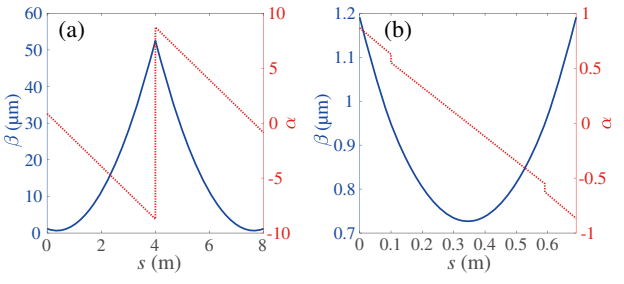

FIG. 14. Longitudinal Twiss matching of two arcs. (a) One rf or laser modulator at the cente.; (b) Two rfs or laser modulators set symmetrically.

Suppose all dipoles in the ring have the same bending radius, namely $\rho_m = \rho$, the radiated synchrotron radiation energy per turn can be written as $U_0 = \frac{e^2\gamma_c^4}{3\varepsilon_0}(\frac{1}{\rho} + \sum \frac{L_u}{4\pi\rho_u^2} + \sum \frac{L_m}{4\pi\rho_m^2})$. Here, the synchrotron radiation in all damping wigglers and all laser modulators is considered. Note that since the electron radiates much smaller energy when accelerated in rfs compared with the bending process in dipoles, rf elements are thought to have no contribution to the longitudinal emittance. Then the longitudinal damping constant is $\alpha_z = U_0/E_c$. We can obtain the equilibrium longitudinal emittance as Eq. (8), with I the summation of all dipoles, undulators, damping wigglers and laser modulators. If only rfs (no laser modulators) appear in a ring, the ultimate equilibrium longitudinal emittance will be

$$\epsilon_z = \frac{11}{48\sqrt{21}} \frac{\lambda_e}{32\pi} \gamma_c^2 \beta_c^2 \theta^3. \quad (29)$$

Here, λ_e denotes electron Compton wavelength. From this expression, ϵ_z is independent of bending radius, but strongly depends on bending angle. Reducing the bending angle of the main dipole can effectively lower the equilibrium longitudinal emittance. It should be noted that this emittance can be very small compared with the longitudinal rf bucket. In the ultimate state, the ring is actually also a weak-focusing one, and such small equilibrium longitudinal emittance contributes to a very long quantum lifetime, even if when the rf is replaced by a laser modulator. However, the circumference of the ring

$$C_{\text{ring}} = 2\pi\rho + \frac{\gamma_c^2 \theta^2 \rho}{30} \left[N_s \theta \left(\frac{2}{3} - \frac{1}{\sqrt[3]{15}} \right) + \pi \right] \quad (30)$$

may be huge, especially for a high energy ring. But if the designed electron beam energy is hundreds of MeV, this value can be reasonable.

If the separation of Eq. (28) is taken to match two arcs, it can be obtained that the minimum longitudinal β-function between the two arcs is $\beta_{\min} \approx \frac{\beta_c^2 \rho \theta^3}{120\sqrt{7}}$. This means an equilibrium energy spread of

$$\sigma_{\delta\text{ring}}^2 \approx \frac{55\sqrt{3}}{48} \frac{\lambda_e}{4\pi} \frac{\gamma_c^2}{\rho}. \quad (31)$$

It is only related with the bending radius. The scaling is $\sigma_{\delta\text{ring}} \propto \rho^{-0.5}$, not that sensitive. Meanwhile, the bunch length at this point is proportional to $\gamma_c \beta_c^2 \theta^3 \sqrt{\rho}$. Reducing the dipole angle can quickly shorten the bunch length.

Table I shows a sample ring working at 400 MeV. The dipoles are relatively small, and maybe more reliable to adopt permanent magnets. With such small bends, the equilibrium longitudinal emittance can be 0.17 pm in the two-rf case. The bunch length will be as short as 0.40 nm.

TABLE I. Parameters of a sample ultimate-longitudinal-emittance ring.

Match strategy	2 rfs
E_c	400 MeV
ρ	1.5 m
θ	61.3 mrad
θ_m	25.0 mrad
L_c	3.53 m
L_{mc}	3.53 m
L_d	1.16 m
U_0	1.51 keV
N_c	12
N_s	8
C_{ring}	385.54 m
Total r_{56}	-3.15 μm
rf voltage V_0	5 MV
Frequency f	500 MHz
h	1.31×10^{-1} m^{-1}
ϕ_s	179.991 deg
ϵ_z	0.17 pm
Energy spread	4.21×10^{-4}
Bucket height	55.00

Such beam is sufficient to produce high-power coherent near-soft-x-ray synchrotron radiation in dipoles or undulators. Besides, under such a small total r_{56}, which is of great challenge to control systems, the ultimate-longitudinal-emittance ring is weak focusing as stated, and the bucket height can be extremely huge. This leads to a very stable microbunch. However, apart from the pressure on the control system, in the ultimate state, there exist some intrinsic issues. The first one is located at the ultralow beam duty cycle due to rf (one single nanometer bunch in every tens of centimeters), whose wavelength is on the order of centimeters. But this situation will be greatly relieved by replacing rfs with laser modulators. The second intrinsic issue originates from the matching of longitudinal Twiss. It is not easy to push electron energy to GeV range, where either the separation between two dipoles will be too large, or the bending angle of dipoles will be too small. To overcome this bottleneck, the ultimate state has to be sacrificed. Namely each dipole has to work at a state that deviates from its IT, and the equilibrium longitudinal emittance or bunch length will hence have an increment.

D. Longitudinal-emittance-minimized storage ring

In the previous subsection, the ultimate longitudinal emittance of a storage ring is presented. For high energy storage ring, this ultimate state means a huge circumference, which is practically impossible. Generally, if any one of the following conditions breaks, the ultimate-longitudinal-emittance state will disappear:

(i) All dipoles between two rfs or laser modulators in the ring have a same IT γ.

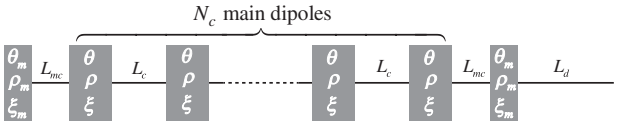

FIG. 15. Layout of a typical longitudinal supercell. Two achromatic dipoles are located at the head and tail, each one has a bending angle of θ_m, radius of ρ_m and r_{56} of ξ_m. N_c main dipoles with separations of L_c are inserted in between. Their bending angle, radius and r_{56} are θ, ρ and ξ respectively. L_d is the space for longitudinal Twiss matching. The total r_{56} of this supercell is ξ_t.

(ii) Separations between dipoles match the IT α and β.

(iii) The setting of rfs or laser modulators does not disturb the longitudinal Twiss in the ring. They are only used for Twiss matching like quadrupoles in the transverse Twiss matching process.

To minimize the equilibrium longitudinal emittance, the optimization of a larger unit, such as one supercell or even the whole ring, should be focused on. Here, we show a method that targets at a super-cell.

Suppose the supercell has a layout shown as Fig. 15, following the analysis of undulator and laser modulator, the 3×3 matrix concatenating method is used to find the entrance longitudinal Twiss of each dipole. Using symbols $(C_{\alpha A}, C_{\beta A}, C_{\gamma A})$, $(C_{\alpha B}, C_{\beta B}, C_{\gamma B})$ and $(C_{\alpha C}, C_{\beta C}, C_{\gamma C})$ for the coefficients of dipole A, B and C respectively, the total coefficients of the supercell will be

$$
\begin{aligned}
C_\alpha &= C_{\alpha A} + C_{\alpha B} + N_c C_{\alpha C} \\
&\quad - N_c \xi_{tc} C_{\beta C} - 2\xi_{tm} C_{\beta B} \\
C_\beta &= C_{\beta A} + C_{\beta B} + N_c C_{\beta C} \\
C_\gamma &= C_{\gamma A} + C_{\gamma B} + N_c C_{\gamma C} \\
&\quad - \frac{1}{2} N_c \xi_{tc} C_{\alpha C} + \xi_{tm}^2 C_{\beta B} - \xi_{tm} C_{\alpha B} \\
&\quad - N_c \left[\xi_{mL}^2 - \xi_{tc} \xi_{mL} - \frac{2Nc - 1}{6(N_c - 1)} (2\xi_{mL} - \xi_{tc})^2 \right] C_{\beta C}.
\end{aligned}
$$

Here, $\xi_{tc} = \xi_t - \xi - \frac{L_d}{\gamma_c^2}$, $\xi_{tm} = \xi_t - \xi_m - \frac{L_d}{\gamma_c^2}$ and $\xi_{mL} = \xi_m + \frac{L_{mc}}{\gamma_c^2}$. The longitudinal Twiss matching using a separation requires that $\xi_t \equiv 0$. With these definitions, parameters can be chosen to satisfy the IT of this supercell, and once done, the longitudinal emittance contribution will be minimized. It is obvious that this IT is not consistent with that of each dipole, which means the dipole's ultimate-longitudinal-emittance state, or Eq. (12), is broken. But usually, for the lattice symmetry, the property $\eta' = 0$ at the center of each main dipole should be kept, which is much easier for operation. It should be pointed out that though the ultimate state is sacrificed, the equilibrium longitudinal emittance can also be orders of magnitude smaller than present electron storage rings, reaching pm to nm range.

TABLE II. Parameters of a sample longitudinal-emittance-minimized ring.

Match strategy	2 laser modulators
E_c	400 MeV
ρ	1.0 m
θ	106.70 mrad
θ_m	43.45 mrad
L_c	3.50 m
L_{mc}	3.50 m
L_d	13.15 m
N_c	9
N_s	6
U_0	2.32 keV
C_{ring}	272.88 m
Total r_{56}	-39.97 μm
Laser strength a_0	1.0×10^{-5}
Laser wavelength λ	1.0 μm
Modulator periods N_u	10
ϵ_z	1.38 pm
Bunch length	3.10 nm
Bucket height	4.24×10^{-2}

Again, for such a small longitudinal emittance, if rfs are taken to match the longitudinal Twiss and compensate energy loss, the relative large rf wavelength will lead to a small duty cycle. Thus, it is preferred to use a device with much smaller modulation wavelength—the laser modulator. Here, we show a sample ring targeting at ultrashort bunch length and taking advantage of laser modulators in Table II. Compared with the ultimate-longitudinal-emittance case in Table I, the dipoles can be larger, and the circumference can also be much shorter. The energy spread is about 4.48×10^{-4}, hence the beam can stay happy in the bucket with a height of 4.24×10^{-2}. Figure 16 presents the longitudinal Twiss functions of this sample ring. As previously stated, the β-function inside dipoles varies a lot. The laser modulator is located around $s = 45$ m. It is originally a drift section, but to keep the longitudinal Twiss matched, when the laser modulator is set, the separation must be adjusted. Around the position of $s = 87$ m and $s = 136$ m, straight sections are prepared for undulators, through which coherent EUV can be produced.

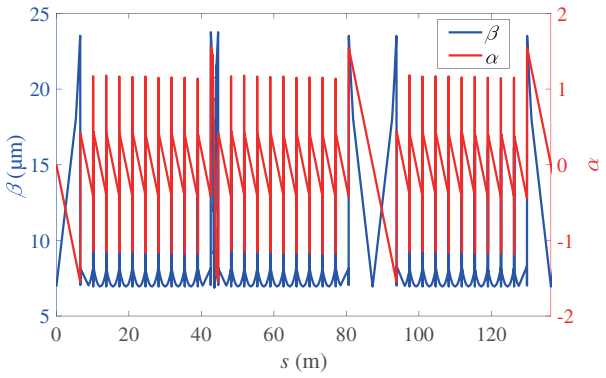

FIG. 16. Longitudinal Twiss functions of the half ring in Table II.

V. CONCLUSION

Decades of studies have focused on the storage ring transverse dynamics, but recently, with the development of storage ring FEL, laser-driven storage ring, SSMB, etc., there is an increasing demand for low or ultralow equilibrium longitudinal emittance. In this paper, the longitudinal Twiss functions are used to analyze the longitudinal dynamics and emittance, imitating the transverse counterparts. The storage ring one-turn map in 3D Twiss form is deduced. According to this form, it is not necessary to remove rf kicks first when analyzing a planar lattice. The dispersion, three-dimensional Twiss and tune can be directly obtained from the one-turn map. This simplifies the analyzing process and may lead to a new and completed way to look into beam dynamics. Making use of this form and based on the longitudinal Twiss function, the equilibrium longitudinal emittance contribution of dipoles, undulators or wigglers, and laser modulators are also theoretically analyzed in a systematic way. For each kind of bend-related element, there exists an emittance-minimized state when a working Twiss matches its intrinsic Twiss. For undulators, wigglers and laser modulators, such state occurs if the central longitudinal beta inside reaches a minimum value. But for dipoles, the dispersion property makes the situation more complicated. Dipoles are clarified into three kinds, with each one being carefully analyzed. By applying these results, the ultimate-emittance state of typical arcs, such as DBA, TBA and MBA, are given. Further more, after the matching of longitudinal IT of these arcs, a storage ring that reaches an ultimate state of longitudinal emittance is formed. In this state, final equilibrium longitudinal emittance will be proportional to γ^2 and θ^3. By reducing θ to tens of milliradians, the equilibrium longitudinal emittance can be orders of magnitude smaller than the current existing worldwide facilities. However, this ultimate-longitudinal-emittance storage ring is not easy to be applied to GeV range since the required dipoles will be too small and the desired circumference will be huge. Compromise has to be made to solve this issue, that is minimizing the longitudinal emittance of a longitudinal supercell. At last, two groups of sample parameters are given to show these longitudinal-emittance-minimized storage rings. Both in the ultimate and longitudinal-emittance-minimized case, to keep the low longitudinal emittance property, a variation of one-turn r_{56} below one micron is required, which is of great challenge for the current control system, but may be available in the next decades.

The design of ultralow longitudinal emittance rings has actually at least two directions, ultralow energy spread and ultrashort bunch length. The former, once combined with

storage ring FEL, can greatly improve the radiation quality and shorten the undulator length. The latter will be of great benefit to the improvement of short wavelength radiation power. Meanwhile, this low longitudinal emittance design is inevitable in the future completely laser-driven storage rings, such as SSMB.

ACKNOWLEDGMENTS

The authors owe much thanks to other Tsinghua colleagues for the discussions. This work is supported by the Tsinghua University Initiative Scientific Research Program No. 20191081195, and the National Natural Science Foundation of China (NSFC Grant No. 12035010).

[1] L. C. Teng, Fermilab Report No. TM-1269, 1984, https://lss.fnal.gov/archive/test-tm/1000/fermilab-tm-1269.pdf.
[2] M. Eriksson, J. F. van der Veen, and C. Quitmann, J. Synchrotron Radiat. **21**, 837 (2014).
[3] L. Liu and H. Westfahl Jr., in *Proceedings of the 8th International Particle Accelerator Conference (IPAC2017), Copenhagen, Denmark, 2017* (JACoW, 2017), p. 1203, http://accelconf.web.cern.ch/ipac2017/papers/tuxa1.pdf.
[4] C. L. Li, C. Feng, and B. C. Jiang, Phys. Rev. Accel. Beams **23**, 110701 (2020).
[5] Z. Huang, K. Bane, Y. Cai, A. Chao, R. Hettel, and C. Pellegrini, Nucl. Instrum. Methods Phys. Res., Sect. A **593**, 120 (2008).
[6] C. Feng and Z. T. Zhao, Sci. Rep. **7**, 4724 (2017).
[7] M. R. Jalal and F. Aghamir, Phys. Lett. A **375**, 1796 (2011).
[8] J. S. Nodvick and D. S. Saxon, Phys. Rev. **96**, 180 (1954).
[9] M. Sands, SLAC Technical Report No. SLAC-121, 1970, https://www.slac.stanford.edu/pubs/slacreports/reports02/slac-r-121.pdf.
[10] F. Wang, D. Cheever, M. Farkhondeh, W. Franklin, E. Ihloff, J. van der Laan, B. McAllister, R. Milner, S. Steadman, C. Tschalaer, D. Wang, D. F. Wang, A. Zolfaghari, T. Zwart, G. L. Carr, B. Podobedov, and F. Sannibale, Phys. Rev. Lett. **96**, 064801 (2006).
[11] M. Abo-Bakr, J. Feikes, K. Holldack, P. Kuske, W. B. Peatman, U. Schade, G.Wustefeld, and H.-W. Hubers, Phys. Rev. Lett. **90**, 094801 (2003).
[12] J. Feikes, M. von Hartrott, M. Ries, P. Schmid, G. Wustefeld, A. Hoehl, R. Klein, R. Muller, and G. Ulm, Phys. Rev. Accel. Beams **14**, 030705 (2011).
[13] Y. Shoji, H. Tanaka, M. Takao, and K. Soutome, Phys. Rev. E **54**, R4556 (1996).
[14] X. J. Deng, A. W. Chao, J. Feikes, W. H. Huang, M. Ries, and C. X. Tang, Phys. Rev. Accel. Beams **23**, 044002 (2020).
[15] D. F. Ratner and A. W. Chao, Phys. Rev. Lett. **105**, 154801 (2010).
[16] Y. Jiao, D. F. Ratner, and A. W. Chao, Phys. Rev. Accel. Beams **14**, 110702 (2011).
[17] S. Khan, Nucl. Instrum. Methods Phys. Res., Sect. A **865**, 95 (2017).
[18] C. X. Tang, X. J. Deng, W. H. Huang, T. H. Rui, A. W. Chao, J. Feikes, J. Li, M. Ries, A. Hoehl, D. F. Ratner, E. Granados, C. Feng, B. C. Jiang, and X. F. Wang, in *Proceedings of the 60th ICFA Advanced Beam Dynamics Workshop on Future Light Sources (FLS2018), Shanghai, China 2018* ((JACoW, 2018), p. 166, https://accelconf.web.cern.ch/fls2018/.
[19] X. J. Deng, A. W. Chao, J. Feikes, A. Hoehl, W. H. Huang, R. Klein, A. Kruschinski, J. Li, A. Matveenko, Y. Petenev, M. Ries, C. X. Tang, and L. X. Yan, Nature (London) **590**, 576 (2021).
[20] E. D. Courant and H. S. Snyder, Ann. Phys. (N.Y.) **3**, 1 (1958).
[21] C. Biscari, Phys. Rev. ST Accel. Beams **8**, 091001 (2005).
[22] A. W. Chao, *Lectures on Accelerator Physics* (World Scientific, Singapore, 2020), http://refhub.elsevier.com/S0168-9002(21)00632-X/sb46.
[23] A. W. Chao, J. Appl. Phys. **50**, 595 (1979).
[24] A. W. Chao, Chin. Phys. C **33**, 115 (2009).
[25] Y. Shoji, Phys. Rev. ST Accel. Beams **7**, 090703 (2004).
[26] F. C. Iselin, Report No. CERN/SL/92, http://mad8.web.cern.ch/mad8/doc/phys_guide.pdf.
[27] Z. Pan, A. W. Chao, X. J. Deng, W. H. Huang, T. Rui, C. X. Tang, W. S. Wan, and Y. Zhang, in *Proceedings of FEL2019, Hamburg, Germany 2019* (JACoW, 2019), p. 700, http://accelconf.web.cern.ch/fel2019/papers/thp055.pdf.
[28] H. Wiedemann, Nucl. Instrum. Methods Phys. Res., Sect. A **266**, 24 (1988).
[29] J. P. Duris, P. Musumeci, and R. K. Li, Phys. Rev. ST Accel. Beams **15**, 061301 (2012).
[30] C. M. S. Sears, E. R. Colby, B. M. Cowan, R. H. Siemann, J. E. Spencer, R. L. Byer, and T. Plettner, Phys. Rev. Lett. **95**, 194801 (2005).